

Broad-area laser diodes with on-chip combined angled cavity

Zefeng Lu (卢泽丰)^{1,2}, Lijie Wang (汪丽杰)¹, Zhide Zhao (赵智德)³, Shili Shu (舒世立)¹,
Guanyu Hou (侯冠宇)^{1,2}, Huanyu Lu (陆寰宇)^{1,2}, Sicong Tian (田思聪)¹,
Cunzhu Tong (佟存柱)^{1,*}, and Lijun Wang (王立军)¹

¹State Key laboratory of Luminescence and Application, Changchun Institute of Optics, Fine Mechanics and Physics, Chinese Academy of Sciences, Changchun 130033, China

²University of Chinese Academy of Sciences, Beijing 100049, China

³Suzhou Everbright Photonics Co., Ltd, Suzhou 215000, China

*Corresponding author: tongcz@ciomp.ac.cn

Received March 14, 2017; accepted May 18, 2017; posted online June 6, 2017

Broad-area diode lasers usually supply high output power but low lateral beam quality. In this Letter, an on-chip combined angled cavity is proposed to realize narrow lateral far field patterns and high brightness. The influence of included angles, emitting facets on output power, and beam quality are investigated. It demonstrates that this V-junction laser is able to achieve a single-lobe far field at optimal cavity length with a 3.4 times improvement in brightness compared with Fabry-Perot (F-P) cavity lasers. The excited high-order modes at a high injection level reduce the brightness, but it is still 107% higher than that of F-P lasers.

OCIS codes: 140.3070, 140.5960, 140.3295, 140.3298.

doi: 10.3788/COL201715.081402.

Semiconductor diode lasers are widely used in a variety of applications, such as pumping^[1], telecommunication^[2], laser display^[3], industrial manufacturing^[4], and medical treatments^[5] because of their high wall-plug efficiency, high reliability, low cost, and small size. The output power of a laser diode is in direct proportion to the area of the gain medium, thus, the most effective and simplest way to realize the high output power is to utilize the broad-ridge waveguide, which is able to scale the power of a near-infrared single-chip diode laser up to 25 W^[6] and support the prosperity of commercial high-power diode lasers and fiber lasers^[7]. However, a broad-area waveguide also leads to a poor lateral beam quality and low brightness. For pumping or direct diode laser purposes, high-power and high beam quality are always desired. Several approaches had been proposed to improve the beam quality and output power, such as unstable resonators with a cured or tilted mirror^[8,9], tapered lasers^[10], angled-grating distributed feedback (DFB) lasers^[11], photonic crystal lasers^[12], curved waveguide lasers^[13], and microstructures integrated on waveguides^[14,15]. These approaches show their advantages, but also with some limitations. The angled cavity^[16-21] was a promising idea, and the corresponding broad-area lasers had demonstrated the high-brightness and single-lobe far field (FF), which was attributed to the mode control of the tilted waveguide and supplied a simple and robust solution for power scaling with good beam quality. The other approach to improve the brightness of diode lasers was the on-chip combining based on the Y-junction tree array^[22] or V-junction resonators^[23,24]. The Y-junction resonator was used to make up a complex tree array to realize the power scaling efficiently, while the V-junction was integrated with angled-grating for

coherent beam combining^[23,24]. The intrinsic reasons for the success of the above methods are the mode suppressing by the tilted waveguide and beam combining on-chip. However, the simple and low-cost fabrication is crucial for the volume production and commercialization. The angled-grating and tree array will increase the difficulty for the realization of high yield and, hence, increase the cost.

In this Letter, we combined the intrinsic characteristics of tilted waveguide and on-chip beam combining and applied the V-junction angled cavity (VAC) with an optimized angle and length on the high-power diode lasers. This type of device was capable of both high-power and high beam quality performance and easily balanced the contradictions between the tilted angle and the waveguide width for the conventional angled cavity. The angle and current dependent beam quality were analyzed, and the lasing spectra were discussed.

Figure 1(a) shows the schematic diagram of the broad-area VAC. It consists of two joint tilted waveguides with an included angle θ , where the width of each waveguide is W . The facet of intersection was labeled as facet 1, and the other facets in the opposite direction were labeled as facet 2. There exists an optimal cavity length for VAC lasers with single-lobe FF and stable resonance along the zigzag paths, which can be expressed as^[18]

$$L = 2mW \cos(\theta/2) / \tan(\theta/2), \quad (1)$$

where m is a positive integer, and $2m$ indicates the counts of the reflection by the ridge sidewalls. In the realistic devices, the optimized cavity length is obtained from Eq. (1).

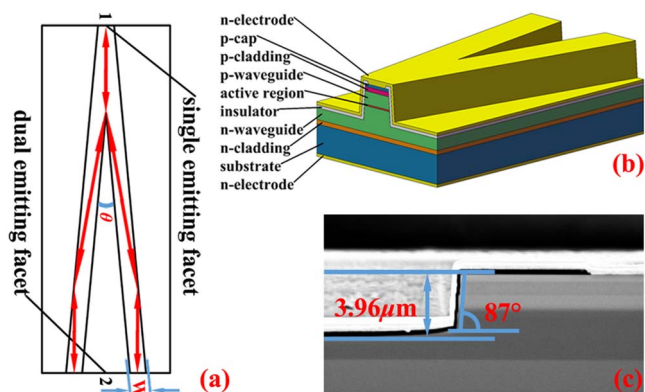


Fig. 1. (a) Schematic diagram of the VAC, (b) the structure of the VAC laser, and (c) SEM image of the emitting facet showing the etching depth and the tilted angle of the ridge sidewall.

Figure 1(b) shows the structure of the VAC laser. The epitaxy structure was grown on $n+$ GaAs substrate with two InGaAs/GaAs quantum wells (QWs), emitting at 960 nm by metal organic chemical vapor deposition (MOCVD). The active region was embedded in an asymmetric waveguide of a super-large optical cavity (SLOC) consisting of 3.0 and 0.4 μm n - and p -doped $\text{Al}_{0.1}\text{Ga}_{0.9}\text{As}$ waveguides, respectively. The cladding layers were, respectively, 0.5 and 0.85 μm $\text{Al}_{0.25}\text{Ga}_{0.75}\text{As}$ in the n - and p -doped side. The thickness of the heavy p -doped GaAs cap layer was 0.4 μm . The devices with the included angles of $\theta = 10^\circ$ and 15° were fabricated. The waveguide width W was 50 μm and was defined by photolithography and inductively coupled plasma (ICP) etching. Figure 1(c) shows the scanning electron microscope (SEM) image of a cross-section of the fabricated waveguide. The etching depth was about 3.96 μm down to the bottom waveguide layer to provide enough feedback on the optical field. Then, an SiO_2 insulation layer was deposited by plasma-enhanced chemical vapor deposition (PECVD). The contact metal was Ti-Pt-Au on the p -side. After substrate thinning and polishing, n metal AuGeNi-Au was deposited. Finally, the wafer was cleaved into individual diode lasers with the optimized cavity length of 1.15 and 1.50 mm, according to Eq. (1), for the included angles of 10° and 15° , respectively. The VAC lasers with a non-optimal cavity length were also obtained by cleaving for comparing. The laser chips were mounted on heat-sink by indium solder with epi-side down and without facet coating for testing. The laser devices with a Fabry–Perot (F-P) cavity, regarded as the included angle of 0° with the ridge width of 100 μm , were fabricated on the same wafer with the etching depth of 1.14 μm for the purpose of comparison. The VAC was just like one F-P cavity divided into two stripes along the center, so the ridge width of the F-P laser for comparison was twice that of the ridge width of the VAC laser.

Figure 2 shows the measured light-current-voltage (L - I - V) performance of F-P lasers and VAC lasers with different included angles under continuous wave (CW)

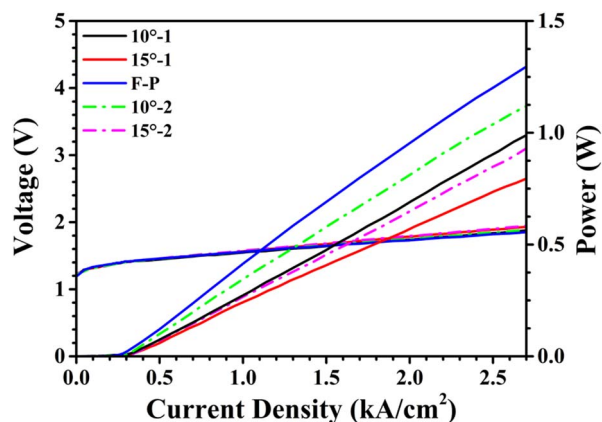


Fig. 2. (Color online) L - I - V performance for on-chip combined angled cavity lasers with different included angles at room temperature under CW operation.

operation at room temperature. Considering the difference of ridge width and optimal cavity length for these devices, the current density was selected as the horizontal axis in Fig. 2 for a more reasonable comparison. As shown in Fig. 2, the threshold current density (J_{th}) increases with the increase of the included angle for VAC lasers, which are respectively 309 and 399 A/cm^2 for the angles of 10° and 15° . These values are higher than the J_{th} of the F-P laser ($\sim 262 \text{ A}/\text{cm}^2$). The homologous result was also found in angled cavity lasers^[19]. One reason for the increased threshold current density is the large mode loss of the transverse mode in the zigzag oscillation^[20,21], while the high reflection (HR) of deep etched sidewalls can improve this situation. The other possible reason behind this might be the suppressed resonance in the angled cavity^[18]. Because of the limitation of the computer, the angled cavity with ridge width $W = 10 \mu\text{m}$, cavity length $L = 92 \mu\text{m}$, and tilt angle $\theta = 12^\circ$ was simulated to support our inference above by MODE Solutions software, and the calculated resonator patterns and facet reflectivity of different-order lateral modes in an angled cavity with optimal cavity length are shown in Fig. 3. Just the fundamental lateral mode and the first-order lateral

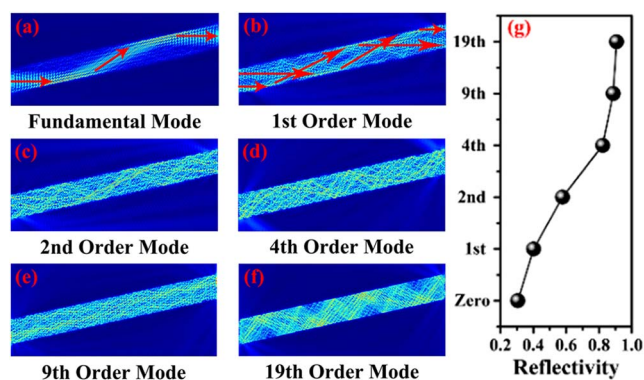


Fig. 3. (Color online) (a)–(f) Calculated resonator patterns and (g) facet reflectivity of different lateral modes in an angled cavity with optimal cavity length.

mode shown in Figs. 3(a) and 3(b) provide the zigzag path clearly, as the red arrows show, however, only the fundamental lateral mode shows the stable resonator pattern inside the angled cavity; the higher-order lateral modes might be emitted like a light emitting diode (LED). The facet reflectivity increases with the increasing number of the lateral modes, and the high energy feedback from the emitting facet and the poor resonator patterns of higher-order lateral modes lead to a higher current density in the angled cavity lasers. In a sense, the emission power might be not the most important factor to comment on these lasers, the beam quality is more crucial. In addition, the efficiencies measured from facet 2 were higher than those from facet 1 for VAC lasers. A similar result was also found in the Y-junction laser array^[22].

The lateral divergences of the above devices under CW operation were measured and plotted in Figs. 4(a) and 4(c) as a function of current density. The lateral FF angles were obtained under the definition of $1/e^2$. It is found that the lateral FF angles increase with the current density, the VAC lasers with an angle of 15° present the lowest values and dependence on the injection, and the variation is less than 1° when the injection increases from 0.5 to 2.7 kA/cm^2 . The FF angles of F-P lasers are also shown in Fig. 4(a) for comparison. The lateral divergence of F-P lasers is between the VAC lasers with angles of 10° and 15° . As can be seen from Figs. 4(a) and 4(b), although the beam quality in the lateral direction worsens at a high current density, the FF of the VAC laser with an optimal cavity length and included angles of 15° and 10° is obviously better than that of the F-P cavity. For the laser beam emitted from facet 2, the profiles show more side-lobes, and the beam quality is much poorer than that from facet 1. In addition, a significant blooming in the FF angle happens at high injected current density. Consider the facts of the better beam divergence from

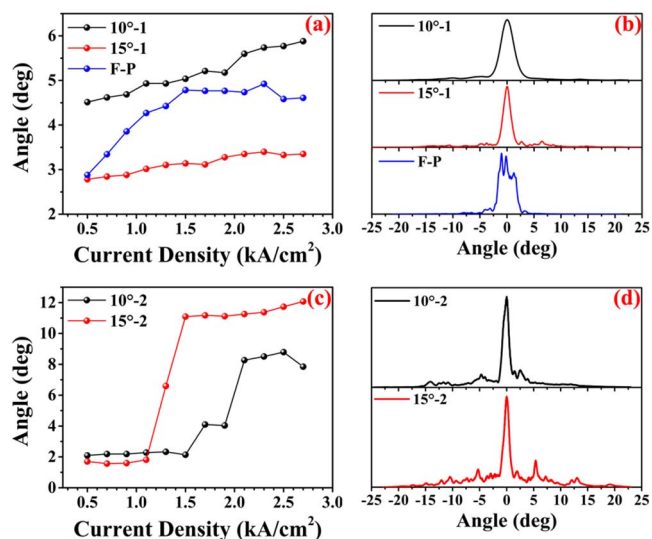


Fig. 4. (Color online) Lateral FF angles as a function of injected current density for emission from (a) facet 1 and (c) facet 2, (b) and (d) are the corresponding lateral profiles at 2.1 kA/cm^2 .

facet 1 and the design purpose of VAC for on-chip combining, the following analysis on the beam quality will only focus on the lasing from facet 1.

Just as mentioned in previous paragraphs, there exists an optimal cavity length for VAC lasers to realize the single-lobe FF. If the cavity length of VAC lasers deviates from the optimized value described by Eq. (1), the FF will worsen. Figure 5 demonstrated this point, in which the lateral FF patterns for the VAC lasers with different cavity lengths are shown. The optimized cavity length for the included angles of 10° and 15° are 1.15 and 1.5 mm, respectively, which shows a single-lobe FF pattern in Fig. 5. For the VAC lasers with a non-optimal cavity length, such as the FF patterns in Fig. 5, the FF is multi-lobe and achieves worse beam quality compared with F-P lasers.

To verify the beam quality of VAC lasers, the beam-waist radius is required, which can be obtained from the near-field (NF). Figure 6 shows the measured beam-waist diameter, which is defined as the $1/e^2$ width of normalized NF intensity. As shown in Fig. 6, the beam-waist of the VAC laser is about three to four times lower than that of F-P laser and shows a weak dependence on the injection. There exists a sudden increase for the beam-waist of the VAC laser in the range from 1.5 to 1.7 kA/cm^2 , where the corresponding value of the beam-waist increases from 25 to over $40 \mu\text{m}$. The measured lasing spectra disclose the possible reason behind it, which is shown in Fig. 7 for VAC lasers with angles of 10° and 15° . As can be seen, the spectrum is broadened and more modes occur at long wavelengths at 1.7 kA/cm^2 , which mean that the growing high-order lateral modes might be responsible for the sudden increase of the beam-waist.

The beam quality is usually described by the beam parameter product (BPP) and the M^2 factor and can be defined as

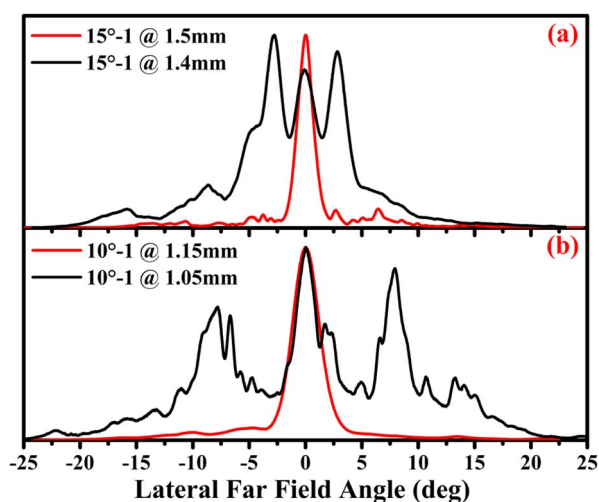


Fig. 5. (Color online) Lateral FF patterns of (a) VAC lasers with angle of 15° and cavity lengths of 1.5 and 1.4 mm, and (b) VAC lasers with angle of 10° and cavity lengths of 1.15 and 1.05 mm at 2.1 kA/cm^2 .

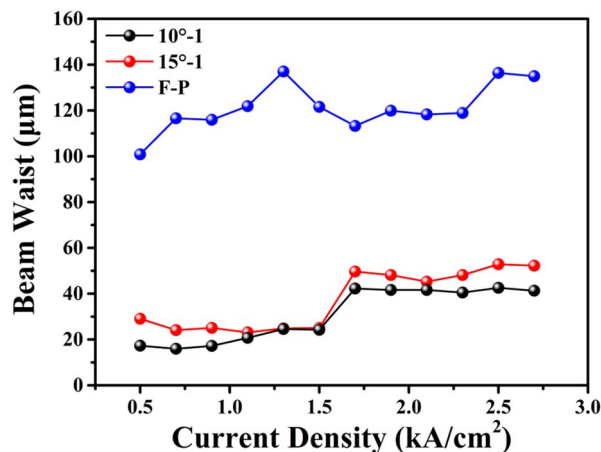


Fig. 6. (Color online) Beam-waist diameter of VAC lasers and F-P lasers under the definition of $1/e^2$ width of normalized NF intensity as a function of injected current density.

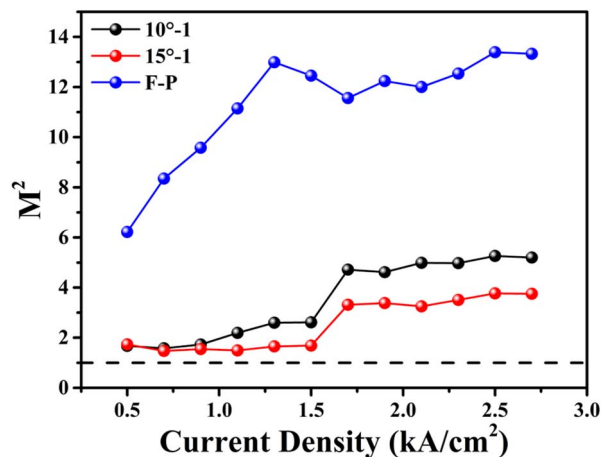


Fig. 8. (Color online) Lateral M^2 factor of VAC and F-P lasers as a function of current density. Dashed line represents the diffraction limit.

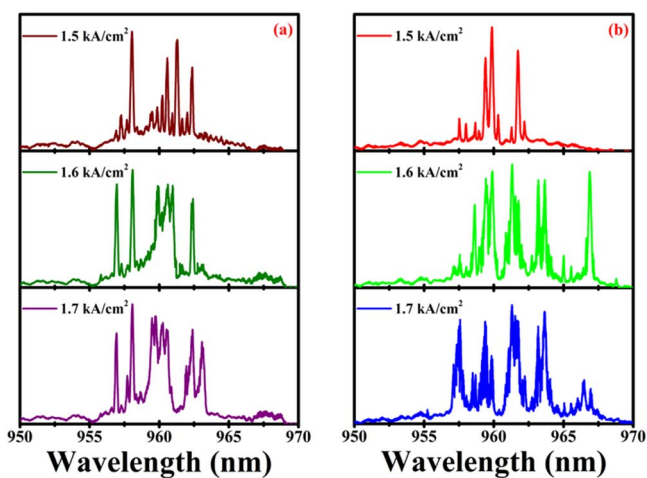


Fig. 7. Lasing spectra of VAC lasers for included angles of (a) 10° and (b) 15° at different injection levels.

$$BPP_{1/e^2} = w_{1/e^2} \theta_{1/e^2} / 4, \quad (2)$$

$$M^2 = BPP_{1/e^2} / BPP_{0-1/e^2}, \quad (3)$$

where $BPP_{0-1/e^2} \approx BPP_0 / 1.5$, and $BPP_0 = \lambda / \pi$, so $M^2 \approx 1.5\pi BPP_{1/e^2} / \lambda$. The factor 1.5 originates from the deviation of selecting the $1/e^2$ definition to describe the beam characteristics^[25]. The w_{1/e^2} in Eq. (2) is the waist diameter at $1/e^2$ of the normalized NF intensity, and BPP_0 is the BPP value of an ideal fundamental mode and only depends on the emitting wavelength. BPP_{0-1/e^2} is the BPP value defined by w_{1/e^2} and θ_{1/e^2} as the diffraction limited beam. Figure 8 shows the current dependent lateral M^2 factor according to Eqs. (2) and (3), where the diffraction limit is labeled as a dashed line. The lateral M^2 factors of the VAC lasers are in the range of 1.47 to 5.27, while on the contrary, the lateral M^2 factor of F-P lasers is as high as 13.4 at a high injection level, which is a typical

value of high-power broad-area diode lasers^[26]. The lateral M^2 factor of the VAC laser with angle of 15° is much better than that of 10° . At a low injection, the lateral M^2 factor of the 15° device is only as low as 1.47, but it degrades to 3.31 after a sudden increase at 1.7 kA/cm^2 , which might be due to the increase of beam-waist resulted by the high-order modes, according to Figs. 6 and 7.

The other important parameter characterizing high-power lasers is the brightness, which shows the trade-off between beam quality and output power, and can be defined as

$$B = P / (\lambda^2 M_x^2 M_y^2), \quad (4)$$

where P is the output power, M_x^2 and M_y^2 are, respectively, the M^2 factor in the x (lateral) and y (vertical) directions. Here, the MODE Solutions software was used to calculate the diffraction limited vertical FF profile of the fundamental mode and compare it with the measured results. The results in Fig. 9(a) show that the vertical FF profiles of the F-P lasers are essentially coincident with the simulated curve (the green dashed line). The difference is that the VAC lasers showed a slightly narrower vertical FF profile because of the 3° tilted ridge sidewalls. The vertical FF angles under the definition of $1/e^2$ were shown in Fig. 9(b). The vertical FF angles were not sensitive to the change of the injection current density, and the variation is less than 1° when the injected current density increased from 0.5 to 2.7 kA/cm^2 . Thus, it is approximated that the beam quality of the y direction was close to the diffraction limit. The brightness of the VAC laser and F-P laser is shown in Fig. 9(c) as a function of current density. At a driving current density of 1.5 kA/cm^2 , the brightness of 19.3 and $26.3 \text{ MWcm}^{-2} \text{ sr}^{-1}$ are, respectively, demonstrated by the VAC laser with the angles of 10° and 15° , which correspond to the improvements of 2.2 and 3.4 times compared with the F-P laser. Although the brightness

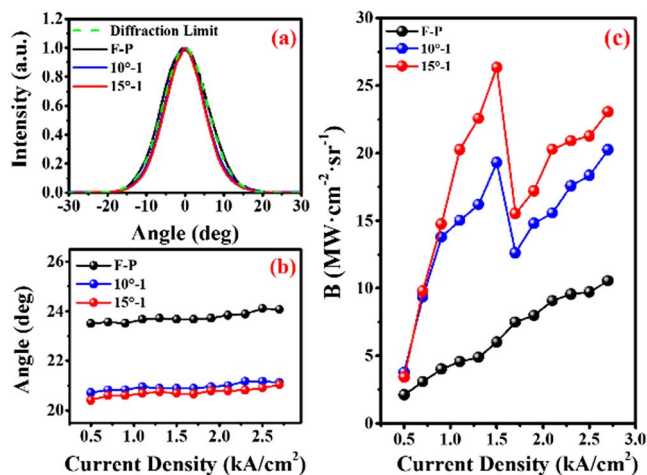


Fig. 9. (Color online) (a) Vertical FF profile of F-P and VAC lasers at 2.7 kA/cm², where the dashed line represents the diffractive limit, (b) vertical FF angles of F-P and VAC lasers as a function of current density, and (c) the brightness of VAC lasers and F-P lasers as a function of current density.

of the VAC laser with an angle of 15° suddenly decreases 41% at 1.7 kA/cm², it is still 107% higher than that of F-P lasers. The above results also reveal the shortcoming of VAC lasers, i.e., high-order modes may be excited and weaken the merits of VAC lasers. To guarantee the realization of higher brightness in a VAC laser, some mode controlling approaches need be applied, such as the microstructure^[14,15] and photonic crystal waveguide^[12]. These approaches should be effective for both the suppressing of high-order modes and the improvement of output power. In addition, if these VAC lasers were coated with anti-reflection (AR) and HR dielectric film at facets 1 and 2, the brightness would be also expected to increase significantly.

In conclusion, the on-chip combined VAC lasers emitting at 960 nm are demonstrated for high beam quality and high-brightness operations. The stable and narrow FF profiles are realized in the devices with an optimal cavity length. A brightness improvement over 3.4 times compared with the F-P lasers is achieved by the VAC lasers with an included angle of 15°. Although the exciting of high-order modes weaken the beam quality, it is still much higher than that of F-P lasers. Considering the incorporation of mode controlling approaches and HR coating, a higher brightness is expected in VAC lasers. We believe these results will contribute to the development of high-brightness broad-area diode lasers.

This work was supported by the National Natural Science Foundation of China (Nos. 61404138 and 61474119), the National Basic Research Program of China (No. 2013CB933303), the International Science Technology Cooperation Program of the Chinese Academy of Sciences (No. 181722KYSB20160005), the International Science Technology Cooperation Program of China

(No. 2013DFR00730), the Jilin Provincial Natural Science Foundation (Nos. 20160101243JC and 20150520105JH), and the Opened Fund of the State Key Laboratory on Integrated Optoelectronics (No. IOSKL2016KF15).

References

- W. J. Kozlovsky and W. P. Risk, *IEEE J. Quantum Electron.* **28**, 1139 (1992).
- S. Zhang, M. G. Boudreau, R. Kuchibhatla, Y. Tao, S. R. Das, E. M. Griswold, and U. Sharma, *J. Vac. Sci. Technol. A* **22**, 803 (2004).
- Y. Gan, Y. Lu, Q. Xu, and C. Q. Xu, *IEEE Photon. Technol. Lett.* **25**, 75 (2013).
- F. Bachmann, *Appl. Surf. Sci.* **208-209**, 125 (2003).
- G. Tam, *J. Clin. Laser Med. Surg.* **17**, 29 (1999).
- V. V. Bezotosnyi, V. Y. Bondarev, O. N. Krokhin, G. T. Mikaelyan, V. A. Oleshchenko, V. F. Pevtsov, Y. M. Popov, and E. A. Cheshev, *Quantum Electron.* **39**, 241 (2009).
- S. Strohmaier, C. Tillkorn, P. Olschowsky, and J. Hostetler, *Opt. Photon. News* **21**, 24 (2010).
- M. L. Tilton, G. C. Dente, A. H. Paxton, J. Cser, R. K. DeFreez, C. E. Moeller, and D. Depatie, *IEEE J. Quantum Electron.* **27**, 2098 (1991).
- S. Ahn, C. Schwarzer, T. Zederbauer, D. C. MacFarland, H. Detz, A. M. Andrews, W. Schrenk, and G. Strasser, *Appl. Phys. Lett.* **104**, 051101 (2014).
- S.-C. Auzanneau, M. Calligaro, M. Krakowski, F. Klopff, S. Deubert, J. P. Reithmaier, and A. Forchel, *Appl. Phys. Lett.* **84**, 2238 (2004).
- K. Paschke, A. Bogatov, F. Bugge, A. E. Drakin, J. Fricke, R. Guther, A. A. Strattonnikov, H. Wenzel, G. Erbert, and G. Trankle, *IEEE J. Sel. Top. Quantum Electron.* **9**, 1172 (2003).
- L. Zhu, X. Sun, G. A. DeRose, A. Scherer, and A. Yariv, *Opt. Express* **16**, 502 (2008).
- R. B. Swint, T. S. Yeoh, V. C. Elarde, J. J. Coleman, and M. S. Zediker, *IEEE Photon. Technol. Lett.* **16**, 12 (2004).
- J. Rong, E. Xing, L. Wang, S. Shu, S. Tian, C. Tong, and L. Wang, *Appl. Phys. Express* **9**, 072104 (2016).
- J. Rong, E. Xing, Y. Zhang, L. Wang, S. Shu, S. Tian, C. Tong, X. Chai, Y. Xu, H. Ni, Z. Niu, and L. Wang, *Opt. Express* **24**, 7246 (2016).
- L. Liu, Y. Liu, H. W. Qu, Y. F. Wang, H. L. Wang, Z. G. Feng, Y. J. Zhang, and W. H. Zheng, *Opt. Lett.* **39**, 2391 (2014).
- L. Liu, H. Qu, Y. Liu, R. Zhang, Y. Zhang, and W. Zheng, *IEEE Photon. Technol. Lett.* **26**, 552 (2014).
- C. H. Tsai, Y. S. Su, C. W. Tsai, D. P. Tsai, and C. F. Lin, *IEEE Photon. Technol. Lett.* **16**, 2412 (2004).
- D. Heydari, Y. Bai, N. Bandyopadhyay, S. Slivken, and M. Razeghi, *Appl. Phys. Lett.* **106**, 091105 (2015).
- Y. Liu, Y. Wang, H. Qu, S. Zhao, L. Li, and W. Zheng, *Appl. Phys. Express* **10**, 032701 (2017).
- Y. Liu, H. W. Qu, S. Y. Zhao, X. Y. Zhou, Y. F. Wang, and W. H. Zheng, *Semicond. Sci. Technol.* **32**, 01LT01 (2017).
- A. Lyakh, R. Maulini, A. Tsekoun, R. Go, and C. K. Patel, *Opt. Express* **22**, 1203 (2014).
- Y. Zhao and L. Zhu, *Opt. Express* **20**, 6375 (2012).
- Z. Yunsong and Z. Lin, *IEEE Photon. J.* **5**, 1500307 (2013).
- O. AB, "Beam parameter product" (Optoskand AB), <http://www.optoskand.se/technology/beam-parameter-product/>.
- R. Hülsewede, J. Sebastian, H. Wenzel, G. Beister, A. Knauer, and G. Erbert, *Opt. Commun.* **192**, 69 (2001).